Fizika Nizkikh Temperatur, 2000, v. 26, Nos. 9/10, p. 863–873

Medium effects on the spectroscopy and intramolecular energy redistribution of C_{60} in cryogenic matrices

M. Chergui

Institut de Physique de la Matiére Condensée, Faculté des Sciences, BSP
Université de Lausanne, CH-1015 Lausanne-Dorigny, Switzerland
E-mail: majed.chergui@ipmc.unil.ch

Received March 22, 2000

We review some of our works on the absorption, excitation and emission spectra of C_{60} embedded in rare gas matrices while stressing the role of the environement. The gas phase resonant two-photon ionization spectrum of C_{60} is reanalysed in the light of our previous work and the energy of the lowest three excited singlet states is determined with precision. In matrices, the visible absorption bands shift red by ~ 30 cm^{-1} in Ne matrices to ~ 330 cm^{-1} in Xe matrices. The observed reversal of state ordering of the lowest two singlets states (T_{1g} and T_{2g}) between Ne and Ar matrices (in emission) and in Ne matrices, between absorption and emission spectra, is attributed to different Stokes shifts of the T_{1g} and T_{2g} states and to the small energy splitting (~ 50 cm^{-1}) between them. Finally, a detailed picture of the intramolecular energy redistribution processes is obtained thanks to a combination of picosecond fluorescence experiments and femtosecond pump-probe transient absorption experiments. The intramolecular relaxation processes among the pure electronic levels of the lowest three singlets states are found to be strongly medium dependent. Even, on the very short time scale of the internal conversion in the singlet vibronic manifold are medium effects manifest.

PACS: 33.20.Lg, 33.50.Dq, 78.40.Ri

1. Introduction

Ever since the large-scale production of fullerenes, there has been a tremendous upsurge of studies concerning them because of their potential applications in different fields. For example, the idea to encapsulate atoms or molecules in fullerenes, i.e., to make endofullerenes, is attractive because of the remarkable properties such systems should exhibit. So far attempts to produce endofullerenes have all been based on «brute force» methods — high intensity laser excitation of metal-coated graphite [1], high temperature ovens [2] or high velocity collisions between fullerene ions and a target gas [3]. None of these methods is selective and efficient. A selective approach would be to use lasers. This requires however a knowledge of the energetics and the energy redistribution processes in these molecule. These data are also of importance in other applications such as optical limiting or the use of fullerenes as saturable absorbers in ultrafast optics [4–6].

According to theory [7,8], the lowest three electronic excited singlet states of C_{60} are the T_{1g}, T_{2g} and G_g states, whose transitions with the ground A_g state are dipole-forbidden. However, these transitions may be vibronically induced by nontotally symmetric modes as a result of Herzberg-Teller (H.-T.) and Jahn-Teller (J.-T.) couplings. The detailed description of these modes and their calculations has mainly been done by Negri and co-workers [7–11]. This raises an additional interesting aspect to fullerenes, which is the possibility to iterate the experimental data with these high quality quantum-chemical calculations [7–11]. As such, C_{60} and C_{70} appear as ideal test systems for improving and refining the quantum chemical calculations of large polyatomic systems.

The ideal situation to determine the energetics would be to study fullerenes in the gas phase. However such studies are not possible, due to the high temperatures needed to vapourize fullerenes and the resulting hot band contributions which arise. Therefore, most of the spectroscopic studies

on fullerenes have mainly been carried out in organic solvents [12,13], in low temperature organic matrices [14–16] and in the pure solid [17,18]. In all these media, the relatively strong interaction of the molecule with the environment leads to a broadening of bands, strong site effects and shifts of the energy levels which make a clearcut assignment of the spectroscopy difficult. Despite this, the first attempt to present a complete assignment of the C_{60} absorption spectrum from the visible to the UV, was made by Leach et al. [12] on data recorded in hexane solvents. In organic Shpolskii matrices, sharp spectra were reported but the large distribution of sites has made a clearcut assignment of bands difficult [14–16]. Another approach is to use molecular beams, which would allow one to have cold, noninteracting molecules, but surprisingly, to our knowledge there has only been one such study in the early days of research on fullerenes [19]. The authors reported on the two-photon resonance enhanced multiphoton ionization of C_{60} and C_{70} in the 600 nm and 400 nm regions but no assignment was proposed of the rich structures therein contained. An alternative approach is to embed the fullerenes in rare gas matrices. The matrix-isolation technique offers a number of advantages.

1). The media are cold (typically < 10 K), so that hot band contributions are suppressed, rotation is hindered and thus the density of occupied states is lowered.

2). The media are chemically inert so that the fullerene molecules interact weakly with them. In the lightest Ne matrix, one should in principle approach the frozen gas phase situation.

3). The rare gas matrix offers a «physical» environment which is ideal to investigate the coupling of the impurity optical transitions to the lattice.

The first study on C_{60} in Ar matrices was undertaken by Gasyna et al. [20] who reported absorption and MCD spectra. Over the past four years, we have undertaken a systematic spectroscopic study of C_{60} and C_{70} in rare gas matrices [21–24]. More recently, we have also looked at their energy redistribution processes [25,26]. Another very promising approach consists in embedding C_{60} in He nanodroplets [27]. This yields absorption (excitation) spectra with richer details than in rare gas matrices, which makes a complete assignment more difficult.

In this contribution, we will review our work on the spectroscopy of C_{60} using the matrix-isolation method with an emphasis on medium effects. We will concentrate however on new aspects either due to as yet unpublished results or to a revised interpretation of already published data. The experimental set-ups and procedures have already been described in Refs. 21–24 and will not be repeated here.

In Sec. 2, we will mainly discuss the absorption spectrum of C_{60} in the visible region. In Sec. 3, we will present and discuss the steady-state fluorescence spectrum of C_{60} in Ne, Ar matrices. This will be completed in Sec. 4 by the time-resolved fluorescence spectroscopy. Section 5 deals with the phosphorescence and Sec. 6 concerns the conclusions.

2. Absorption spectroscopy

Figure 1 compares the resonant two-photon ionization spectrum of C_{60} in molecular beams from Ref. 19, with our excitation and absorption spectra in Ne matrices. The spectra exhibit the same spectroscopic features, except for a red shift and a broadening of bands in going from gas phase to Ne matrices. The same holds for the spectra recorded in heavier matrices (not shown here). In addition, the close resemblance between excitation and absorption spectra suggests that all the absorbing levels lead to fluorescence with the same quantum efficiency. The broadening of bands is mainly due to inhomogeneous broadening (the resolution was ~ 1 cm^{-1} in these spectra). The red shift increases from Ne to Xe as shown in Table 1 (the shifts are averages of those measured on the main bands in Fig. 1).

Table 1

Gas-to-matrix shifts measured on the main bands in the visible absorption spectrum of C_{60} in rare gas matrices

Rare gas	Neon	Argon	Krypton	Xenon
ΔE, cm^{-1}	35 ± 5	160 ± 10	230 ± 20	330 ± 30

In Ref. 22, the fluorescence spectrum of C_{60} in Ar and Ne matrices was precisely assigned, thanks to the high-quality calculations of the vibronic modes and their oscillator strengths in the Jahn-Teller and Herzberg-Teller couplings. The mirror image which we obtained between the excitation spectrum and the fluorescence spectrum in Ar matrices, allowed us also to assign the excitation spectrum. However, it was noted that in using a common pure electronic origin to all excitation bands, the frequencies of the vibronic modes associated to the G_g electronic state were shifted by ~ 60 cm^{-1} to lower energies than their value in the fluorescence spectrum. We recall that these values were in remarkable accord with those calculated [22]. Given that such a change of mode frequencies between

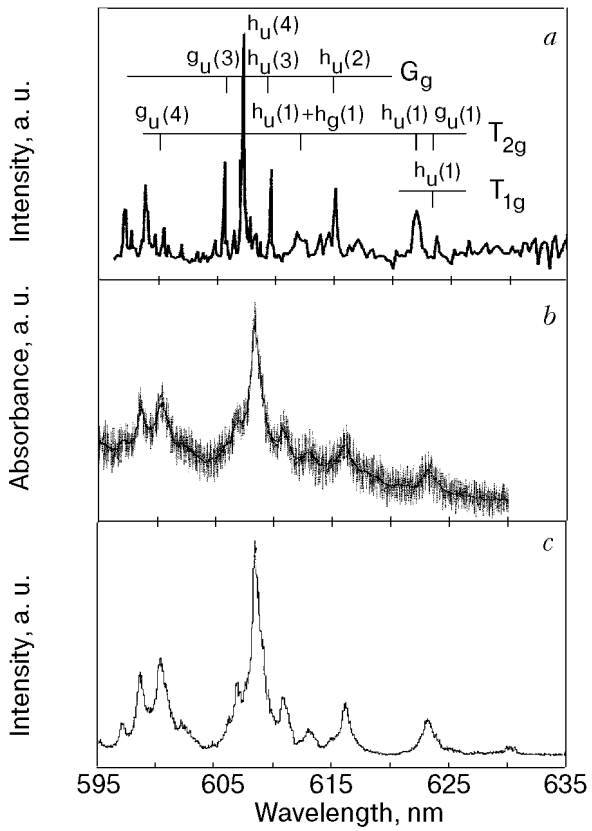

Fig. 1. Comparison the gas phase resonant two-photon ionization spectrum of C_{60} from Ref. 18 (*a*) with the absorption (*b*) and excitation (*c*) spectra of C_{60} in Ne matrices at 4 K.

ground and excited state is unlikely (but not excluded), we proposed that the G_g state should lie ~ 60 cm^{-1} above the T_{1g} and T_{2g} states. The hypothesis of a G_g state lying ~ 50–100 cm^{-1} higher than the T_{1g} and T_{2g} states had already been proposed by Negri et al. [9]. In their case, the assignment of the gas phase spectrum considered only modes associated with the T_{1g} and G_g states. More recently, an energy splitting of ~ 100 cm^{-1} between these states was independently found in temperature-dependent studies of the C_{60} fluorescence in low temperature decalin/cyclohexane matrices [16].

We can now be more precise as, knowing exactly the mode frequencies from the fluorescence spectra and their assignment to the T_{1g}, T_{2g} and G_g states [22], we can trace back the electronic origin of these three states in the gas phase spectrum and the matrix data. The analysis of the gas phase spectrum is given in Table 2 and the attribution of bands is shown in Fig. 1. The gas phase energies of the electronic origin obtained from such a procedure imply that the T_{1g} state is the lowest with an energy of 15632 cm^{-1}, T_{2g} is the next one above at 15681 ± 10 cm^{-1}, and G_g is the third with an energy 15738 ± 10 cm^{-1}. The uncertainty is due to the dispersion of mode frequencies and the pointing of energies in the published gas phase spectrum. In the case of the lowest state and since only one vibronic band can be assigned to it (Fig. 1), we could not give error bars. However, in line with Refs. 9 and 16, we find that the T_{1g}–G_g splitting is indeed ~ 100 cm^{-1}.

Table 2

Band wavelengths and energies of the phase resonant two-photon ionization spectrum of C_{60} from Ref. 19. The assignments are based on the matrix data of Refs. 21, 22.

Wavelength	Energy	Mode	Mode frequency [22]	Electronic state
623.66	16034	$h_u(1)$ /$h_u(1)$	345–352/402	T_{2g} /T_{1g}
621.7	16085	$h_u(1)$	402	T_{2g}
617.2	16027.3			
614.8	16265.4	$h_u(2)$	525–536	G_g
~ 612	16340	$h_u(1)$ /$h_g(1)$	668	T_{2g}
609.4	16409.6	$h_u(3)$	668	G_g
607.1	16471.7	$h_u(4)$	743–738	G_g
605.3	16520.7	$g_u(3)$	776	G_g
604.65	16538.5	$h_u(2) + h_g(1)$	791–802	G_g
601.9	16614			
600.3	16658.3	$g_u(4)$	962	T_{2g}
598.8	16700			
596.9	16753			

The region of the electronic origin in Ne matrices is shown in Fig. 2. Recently, much less noisy contours of the threshold region were obtained for C_{60} in He_n nanodroplets [27], which confirm our results in Fig. 2. The striking feature of this threshold

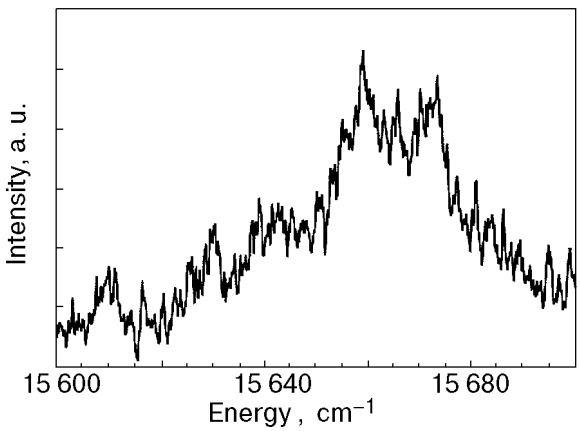

Fig. 2. Threshold region (pure electronic origin) of the visible absorption of C_{60} in Ne matrices.

region, as compared to the higher lying vibronically induced bands, is that the latter are sharp and typically represent zero-phonon lines with no detectable phonon sideband. On the other hand, the threshold region consists of broad structureless features suggestive of a significant electron-phonon coupling for these transitions. Furthermore, as the pure electronic transitions are dipole-forbidden, they must be dynamically induced by the participation of nontotally symetric modes of the cage. The absence of a zero-phonon line for the threshold region and the fact that the bands therein are broad, implies a significant structural rearrangement prior to emission, accompanied by an absorption-emission Stokes shift. We reported in Ref. 21 a Stokes shift of ~ 30 cm^{-1} in Ne matrices and ~ 50 cm^{-1} in Ar matrices, measuring it from the maximum of the absorption threshold to the maximum of the emission origin.

The resemblance between the gas and the matrix data in Fig. 1 shows that the different environments do not affect the oscillator strengths of the different vibronically induced transitions in absorption. In the next Section, we will see that this is not the case for the fluorescence.

3. Fluorescence spectra

Figure 3 shows the experimental and simulated fluorescence spectra of C_{60} in Ne and Ar matrices which were already presented and discussed in detail in Ref. 22, along with the assignment of bands. This assignment was based on the fact that only one single electronic origin appears in the spectra and that the mode frequencies for all three lowest lying electronic states inferred from this origin are in remarkable agreement with the calculated ones. Since the fluorescence spectrum contains vibronically induced transitions which are characteristic of the lowest three electronic states, the S_1 state responsible for the emission has to be a state of mixed T_{1g}, T_{2g} and G_g character. From the simulated spectra, the weighting based on intensities was $T_{1g}:T_{2g}:G_g$ = 36%:56%:8% in Ne matrices and 50%:25%:25% in Ar matrices [22].

The near mirror image between excitation and fluorescence spectra in Ar matrices suggests that the three states responsible for the absorption (see above) may also appear in emission with the same oscillator strengths and relative intensities as in absorption. Yet, aside from being unlikely, this idea is ruled out on the fact that, as mentioned above, our emission spectra clearly show one single electronic origin, i.e., it stems from only one single emitting state. This is also confirmed by the time-

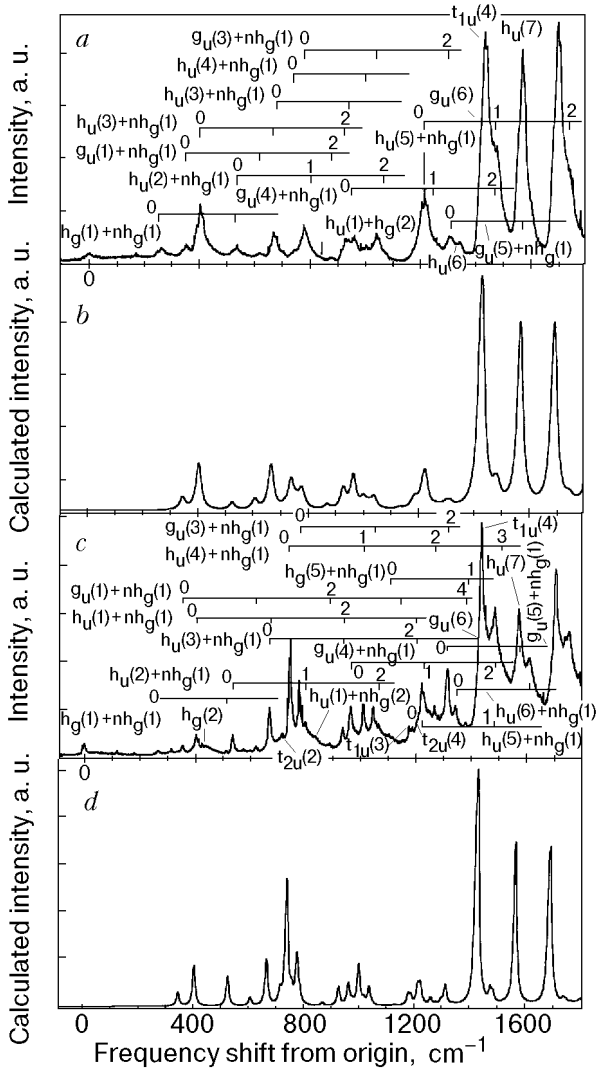

Fig. 3. Fluorescence spectrum of C_{60} in Ne matrices as a function of frequency shift from origin in the 0 to 1600 cm^{-1} region (*a*); simulation of the fluorescence spectrum based on computed oscillator strengths (Ref. 22). The contribution of the T_{1g}, T_{2g} and G_g symmetry characters states to the emission is 36, 56 and 8%, respectively (*b*); same as (*a*) but for Ar (*c*); same as (*b*) but the contribution of the T_{1g}, T_{2g} and G_g symmetry characters to the emission is 50, 25 and 25%, respectively (*d*).

resolved picosecond fluorescence measurements as we will see in Sec. 4. Therefore, even though it helped us assign the excitation (absorption) spectrum in Ref. 22, the resemblance between emission and excitation spectra in Ar matrices is, we believe, fortuitous. Coming back to the differences between the Ne and Ar emission spectra, it is remarkable to note how dramatic is the effect of such supposedly «weakly interacting» media. Indeed, the weighting of intensities implies that the dominant character of the S_1 emitting state switches from T_{1g} in Ar matrices to T_{2g} in Ne matrices, whereas the absorp-

tion spectra indicates that the T_{1g} state is the lowest lying state (Sec. 2). This points to a reversal of state ordering in going from Ar to Ne and in going from absorption to emission. The sole possibility that this could happen is by different absorption-emission Stokes shifts of the T_{1g} and T_{2g} states in the two matrices. As mentioned in the previous section, the purely electronic transitions at the origin are characterized by multiphonon bands implying a sizeable Stokes shift, which brings the energy of the state to lower values. If, for a reason that still needs to be clarified, the Stokes shift is stronger in Ne for the T_{2g} state as compared to that of the T_{1g} state, then the T_{2g} state may end up at an energy slightly lower than the energy of the T_{1g} state, which would explain the reversal of state ordering between the two matrices and between absorption and emission.

The origin of the different mixing ratios between the lowest three pure electronic states may be due to one or a combination of the following factors:

— in going from one matrix to the other, there is a differential shift of $\sim 100\ \text{cm}^{-1}$ (see Table 1) which will modify the resonance conditions between the lowest three singlet states and the nearby triplet state manifold. This might give rise to singlet-triplet couplings which can alter the singlet-singlet mixing among the S_1 to S_3 states. However, if this were the case, then an intersystem crossing from S_2 or S_3 to the T_n states could take place, a hypothesis that is excluded on the basis of the time-resolved data presented in Sec. 4;

— mixing by static symmetry effects: even if we have no idea of the local symmetry of the trapping site, it is clear that it changes in going from Ne to Ar. Indeed, a simple estimate based on Lennard-Jones radii of C_{60} and rare gas atoms shows that 18 Ne atoms and 12 to 13 Ar atoms are needed to cover the surface of C_{60}. This means that there is a lowering of symmetry in going from the gas phase (I_h group symmetry for C_{60}) to Ne to Ar matrices. The lower the symmetry, the higher the likehood to induce state mixings;

— mixing by dynamical symmetry effects: as mentionned in Sec. 2, in order to lift the forbidden character of the pure electronic transitions, nontotally symmetric modes of the cage have to be involved. Likewise, nontotally symmetric modes (having gerade character) can mix the lowest three singlet states with each other and give rise to the mixed character of the S_1 state, in particular given the small energy gaps between them, of typically one phonon energy.

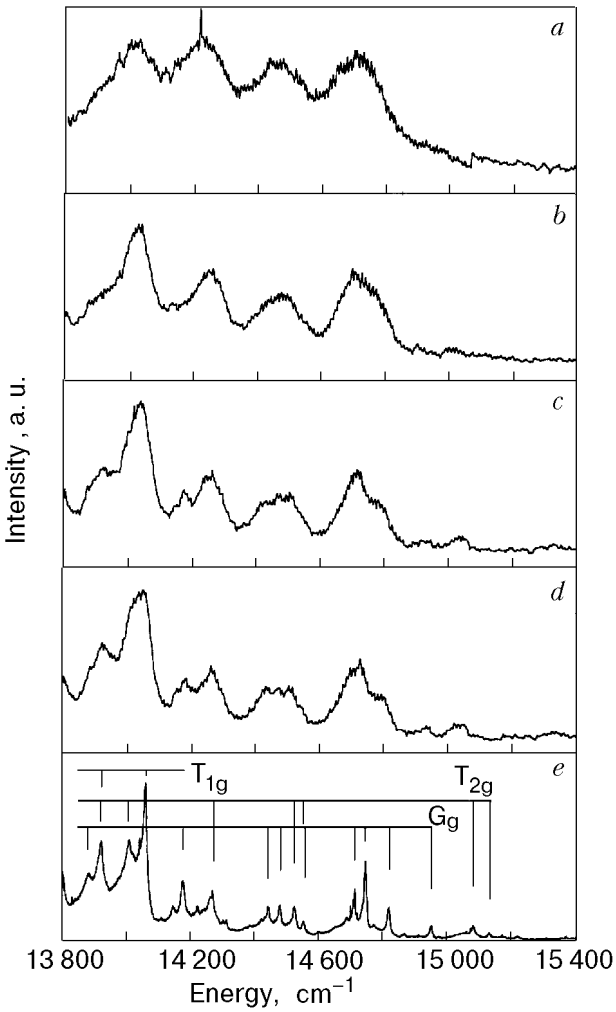

Fig. 4. Time-gated fluorescence spectra of C_{60} in Ar matrices at different τ, ps: 30 (*a*), 90 (*b*), 150 (*c*), 210 (*d*) and under steady-state conditions (*e*).

4. Time resolved fluorescence spectra

In order to identify the intramolecular relaxation pathways leading to the lowest singlet emission and, from there, to the population of triplet states, we carried out picosecond fluorescence measurements in Ne and Ar matrices. The description of the apparatus is given in Ref. 25 along with a detailed presentation of the results. Here, we emphasize the medium effects in the light of the above.

Figure 4 shows typical results in the case of C_{60} in Ar matrices, and represents a set of time-gated fluorescence spectra along with a spectrum recorded under steady state conditions (Fig. 4,*e*) as discussed in Sec. 3. In Fig. 4,*e*, the high frequency region of the spectrum is dominated by a group of bands around $14750\ \text{cm}^{-1}$ which are due to the $h_u(3)$, $h_u(4)$ and $g_u(3)$ modes of the molecules (all have frequencies around $700\ \text{cm}^{-1}$) [22], characteristic of the G_g emitting character. On the other hand, the

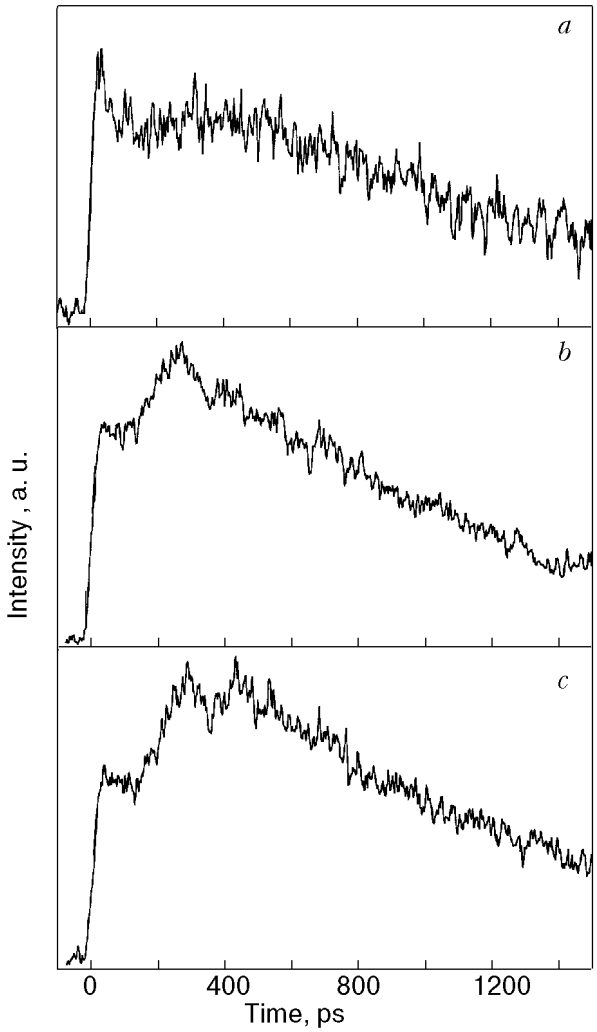

Fig. 5. Time-resolved fluorescence decay of the fluorescence bands of C_{60} in Ar matrices belonging to the different emitting characters: $h_u(4)$ of the G_g character (*a*); $t_{1u}(4)$ of the T_{1g} character (*b*), and $h_u(1)$ of the T_{2g} character (*c*).

bands at ~ 14040 cm^{-1} and ~ 13800 cm^{-1} are due to the $t_{1u}(4)$ and $t_{1u}(4) + h_g(1)$ modes, typical of the T_{1g} emitting character. Finally, the band at ~ 13900 cm^{-1} is due to the $h_u(7)$ mode which is to more than 80% due to the T_{2g} emitting character. If we now consider the time-gated fluorescence spectra (Fig. 4,*a–d*), one can see that the spectrum at 30 ps (Fig. 4,*a*) exhibits a series of broad features of almost equal intensities in the 14800–13900 cm^{-1} region. This means that compared to the steady-state spectrum, the bands at frequencies > 14100 cm^{-1} (most being characteristic of the G_g emitting character) are significantly enhanced as compared to those due to the T_{1g} and T_{2g} emitting characters. In addition, the bands characteristic of the latter two are also of comparable intensity (compare, e.g., the 13900 cm^{-1} band with the 14040 cm^{-1} band). The situation changes however rapidly, as already at 90 ps (Fig. 4,*b*), the bands characteristic of T_{1g}/T_{2g} dominate the spectrum, while all the bands tend to sharpen and the spectrum reproduces most of the features of the steady state spectrum by ~ 200 ps. A line narrowing also occurs which corresponds to a change of line width by a factor of 2 between 30 and 150 ps.

This description of the time-gated fluorescence spectra shows that the bands associated with the G_g and the T_{1g}/T_{2g} characters exhibit nonidentical behaviors in the short time domain (~ 200 ps). This is better visualized by plotting the time-resolved fluorescence decay curves at given emission wavelengths (i.e., looking at a band or group of bands). Time-resolved fluorescence decay curves of C_{60} in Ar matrices are given in Fig. 5, for selected fluorescence bands belonging to each emitting character. The structure at very early times (most visible in Fig. 5,*c*) is due to the scattered laser light and the response of the detection system, as checked by recording the time-profile of the emitted light at a

Table 3

Time constants of the different components of the time-resolved fluorescence spectra of C_{60} in neon and argon matrices. τ_1 represents a decay time in the case of the G_g emitting character, and a rise time in the case of the T_{1g}/T_{2g} emitting characters

Emitting character	Vibronic bands	τ_1, ps	τ_2, ps	Vibronic bands	τ_1, ps	τ_2, ps
	Neon			Argon		
T_{1g}	$t_{1u}(4)$ $t_{1u}(4) + h_g(1)$	205 ± 30	900 ± 150	$t_{1u}(4)$ $t_{1u}(4) + h_g(1)$	90 ± 20	1455 ± 150
T_{2g}	$g_u(6)$, $h_u(7)$ $h_u(7) + h_g(1)$ $h_u(1)$	170 ± 30	875 ± 120	$g_u(4)$, $h_u(5)$ $g_u(4) + h_g(1)$ $h_u(7)$	60 ± 20	1690 ± 200
G_g	$g_u(5)$ $g_u(5) + h_g(1)$	130 ± 30	935 ± 150	$h_u(3)$, $h_u(4)$ $g_u(3)$, $h_g(6)$ $g_u(5)$	60 ± 20	1490 ± 200

position where no emission band occurs (e.g., at ~ 15400 cm^{-1}). It can be seen that the fluorescence associated to the G_g character (Fig. 5,*a*) is characterized by a biexponential decay, with a short component having a decay constant of ~ 70 ps and a long one with a decay constant of ~ 1500 ps. On the other hand, the fluorescence bands associated to the T_{2g} and T_{1g} emitting character (Fig. 5,*b*,*c*) show a short rise followed by a long decay. The rising component has a time constant of ~ 70 ps, while the long decay component has a time constant also of ~ 1500 ps. In the case of Ne matrices, we observe a similar behavior except that the time constants are different. The time constants, given by a fit with a biexponential function, are given in Table 3 for both matrices. It is clear that the decay times of the long component are identical for all vibronic bands attributed to the three different emitting character. Therefore, the hypothesis of a single emitting S_1 state which consists of a mixed T_{1g} , T_{2g} and G_g character is further confirmed. On the other hand, the short time behavior suggests the existence of a short-lived transient fluorescence of dominant G_g character that feeds the S_1 fluorescence. This point is discussed further below.

In summary, our results show that:

a) all emission bands exhibit the same decay rate of ~ 0.9 ns in Ne and ~ 1.5 ns in Ar, indicating that only one emitting S_1 state of mixed T_{1g} , T_{2g} and G_g character, is responsible for the steady state fluorescence spectra;

b) in the 30–100 ps time domain, the fluorescence bands belonging to the G_g emitting character are enhanced in Ne and Ar, relative to later times. In Ne, they remain however weaker than the bands belonging to the T_{2g} and T_{1g} emitting characters, while in Ar at 30 ps, they are equally as strong;

c) the observations in b) are corroborated by the time-resolved fluorescence spectra of the various bands. In Ne and Ar matrices, the bands belonging to the G_g emitting character are characterized by a short decaying component having a time constant ~ 170 ± 40 ps for Ne and ~ 70 ± 20 ps in Ar (Table 3). Those belonging to the T_{1g} and T_{2g} emitting characters exhibit, on the other hand, a rising component having a similar time constant in the respective matrices;

d) there is a significant narrowing of the spectral lines within the first 100 ps or so, but the line widths become essentially constant beyond ~ 200 ps in Ne and ~ 90 ps in Ar.

The ultrafast relaxation from the initially excited state S_n to the S_3 level has in the meantime been measured in the femtosecond domain using pump-probe transient absorption. It was found to occur in ~ 500 fs in Ar matrices [26]. The similarity between absorption and excitation spectra (Fig. 1) clearly suggests that this process is an internal conversion (IC) involving only the excited singlet vibronic states. However differences between Ne and Ar matrices for this ultrafast IC relaxation process were found and are being investigated in more detail at present [28]. Coming back to the relaxation processes between the lowest three singlet states, the time-resolved data was discussed in Ref. 25, where we assumed that the S_3 state of dominant G_g character relaxes to the nearly degenerate S_1/S_2 states having dominant T_{2g} and T_{1g} characters. The latter depends on the matrix as discussed in the preceding paragraph. We assumed the S_3 state to lie ~ 50 cm^{-1} above the S_2/S_1 state on the basis of the absorption data only, however in line with the above discussion (see Sec. 2), a value of ~ 100 cm^{-1} would be more realistic. Nevertheless, the quantitative details of the relaxation process are not important. What is crucial here is that, in line with the discussion in Sec. 3, static crystal field effects and/or nontotally symmetric modes of the cage need to be involved in order to couple the G_g state with the T_{1g} and T_{2g} states. Consistent with the steady-state fluorescence data, the time-resolved ones confirm that such effects are stronger in Ar than in Ne matrices, probably because of the lower local cage symmetry in Ar.

On the basis of our picosecond fluorescence data and our preliminary femtosecond transient absorption measurements, we may already draw a general picture of the ultrafast intramolecular energy redistribution. Following excitation of the S_n state (or group of states) by the UV pump pulse, intramolecular S_n–S_3 relaxation occurs on an ultrafast time scale of a few hundreds of femtosecond. This is a remarkably short time scale for the dissipation of over 1 eV of energy by internal conversion. We stress once more that in this picture, coupling of the singlet vibronic levels with resonant levels of the triplet manifold or the ground state is excluded. In the first case, the intersystem crossing time of about 1 ns for the S_1 state shows that it is a very inefficient process to compete with IC. In the second case, the Franck-Condon overlap integrals of the singlet vibronic levels with the ground state vibrational levels should be negligibly small [7–11]. Finally, such processes are state selective and the similarity between absorption and excitation spectra (Fig. 1) rules out such a selectivity. From S_3 , the population decays to S_2 /S_1 in tens of picoseconds as it is mediated only by lattice phonons.

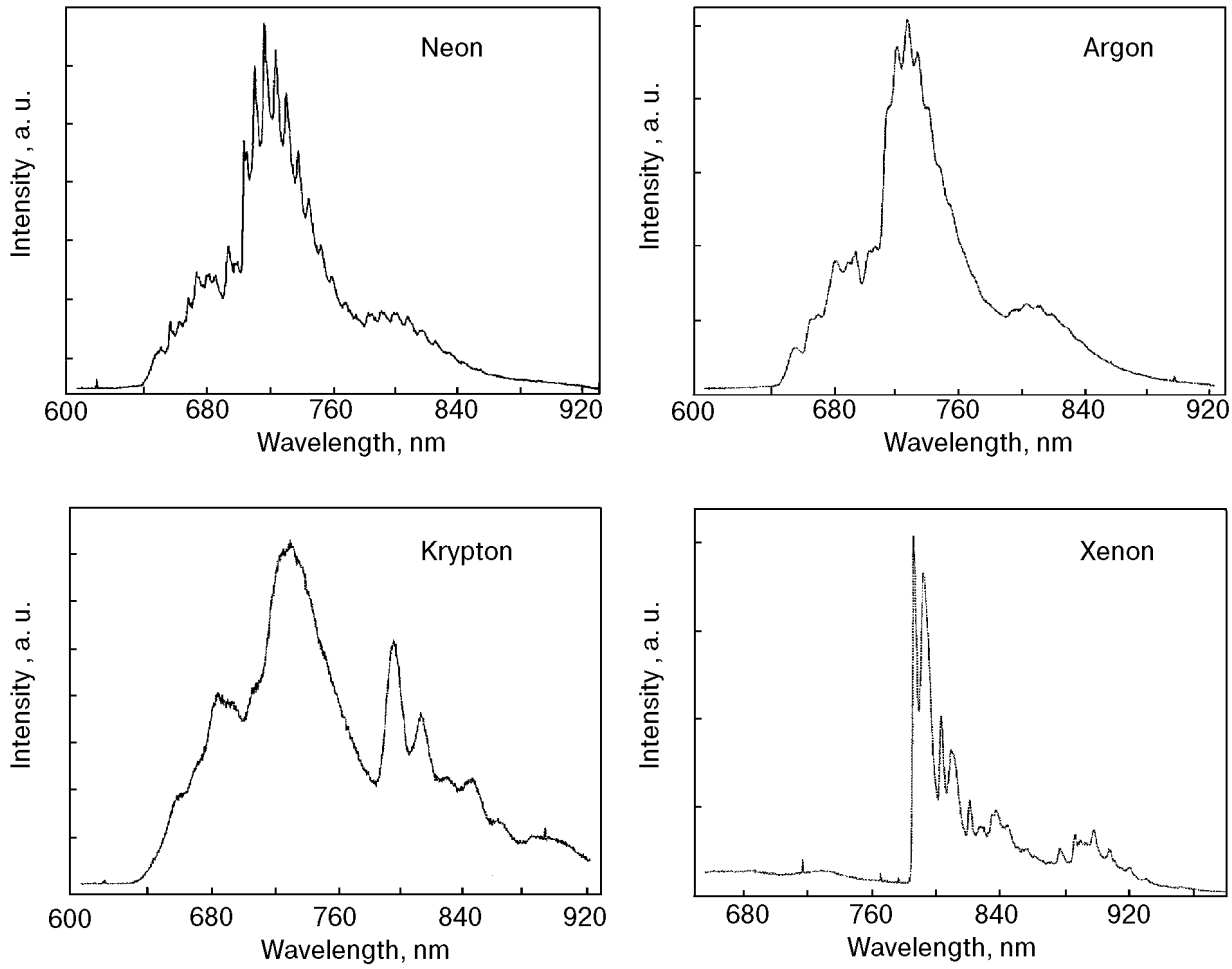

Fig. 6. Overwiew of low resolution emission spectra of C_{60} in Ne, Ar, Kr and Xe. Note the broadening of fluorescence bands and the appearance of new bands on the red side of the spectrum, in going to heavier matrices.

From S_1, intersystem crossing then occurs on the timescale of 1 ns. Note however that even in this case, we also see a medium dependence (Table 3) which should, in our opinion, be due to resonance conditions of S_1 with the triplet levels and/or of the changing dominant symmetry character of S_1. Internal conversion within the triplet manifold should again proceed on an ultrafast time scale followed by a tens of μs radiative decay to the ground state [25] (see Sec. 5).

5. Phosphorescence spectra

In going to heavier matrices, such as Kr or Xe, the medium effects become more striking. The singlet emission bands broaden significantly and tend to decrease in intensity at the expense of new emission bands on the red side, as seen in Fig. 6. These new emission bands are phosphorescence bands which are attributed to the triplet states of C_{60}. A detailed discussion and assignment was presented in Ref. 24 in the case of Xe matrices. We found that site effects are dramatic in such media, resulting in energy differences of ~ 100 cm^{-1} between trapping sites. Furthermore, these sites are stable against annealing up to 50 K and in both, lifetimes of ~ 15 μs are measured.

A detailed analysis of the phosphorescence spectra in Xe matrices was carried out which is presented in Fig. 7 and in Table 4. The spectrum shows two groups of bands belonging to different sites. If we consider the progression with an origin at 786.5 nm which is due to the main site and on the basis of the mode frequencies determined from the fluorescence spectra of C_{60} in Ne and Ar matrices [22], we can assign all the peaks to H.-T. modes of g_u, h_u, t_{1u} or t_{2u} symmetry, in addition to the dominant J.-T. $h_g(1)$ mode, and to combination modes with the latter. With the T_{1g} symmetry of the spin-orbit operator, all these modes can vibronically induce phosphorescence from any of the lowest three triplet states $^3T_{1g}$, $^3T_{2g}$ and ^3G_g, to the ^1A_g ground state. According to Negri et al. [6] and László et al. [29] the lowest triplet state is the $^3T_{2g}$ state whereas the $^3T_{1g}$ and ^3G_g lie about

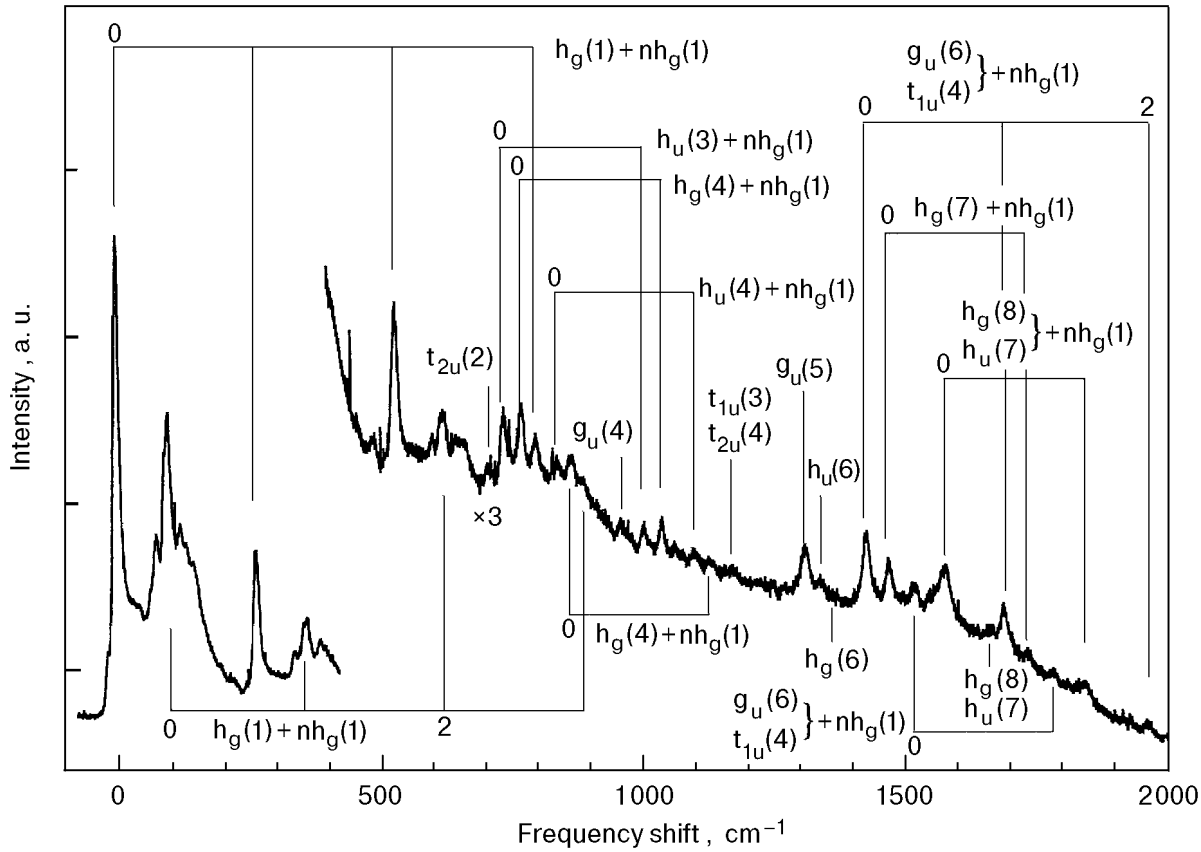

Fig. 7. High resolution ($\Delta\lambda = 2$ Å) phosphorescence spectrum of the 780–950 nm region of C_{60} in Xe matrices ($\lambda_{exc} = 500$ nm), plotted as a function of the frequency shift from the first band at 786.5 nm. The top assignments are those of the 786.5 nm progression (site I in Table 4) and the bottom assignments are those of the 792.5 nm progression (site II in Table 4).

0.3 eV and 0.6 eV higher in energy, respectively. This assignment of the lowest triplet state seems to allow a consistent interpretation of the triplet-triplet absorption spectra [30]. In our phosphorescence spectra, the absence of a_u modes (expected for the $^3T_{1g}$ state) and of g_g modes (expected for the ^3G_g state) support the assignment of the lowest triplet state as $^3T_{2g}$.

The energy ordering of the triplet states as T_{2g}, T_{1g}, G_g is in line with the ordering of singlet states in the emission spectrum in Ne matrices, but differs from that observed in Ar. It also differs from the one observed in the absorption spectra of the singlet states (Sec. 2). In the case of C_{70} in Ne matrices, for which we could clearly separate the different origins of the lowest singlet electronic states, we observed that the ordering of state symmetries between S_1 and S_2 (separated by ~ 260 cm^{-1}) was the same in absorption and in emission [23]. Furthermore, the energy splittings between the S_1 and S_2 states and ordering of states was found to be the same for the lowest two triplet states, T_1 and T_2. Therefore in C_{60}, either the ordering of the triplet states differs from that of the singlet states as suggested by theory [28,29] or, as discussed in Sec. 3 for the singlet states, it would seem that the lowest triplet state also undergo a reversal of state ordering. The reversal in the case of C_{60} in rare gas matrices is probably due to the small energy splitting between the lowest electronic states (~ 50 cm^{-1}) which is of the order of the absorption-emission Stokes shift they undergo.

It is interesting to note that contrary to fluorescence, phosphorescence is dominated by the Jahn-Teller $h_g(1)$ mode while, all the other J.-T. or H.-T. bands are weaker by at least one order of magnitude. This suggests that a coupling mediated by these modes is probably very weak due to the fact that the surfaces associated to them are strongly shifted with respect to the equilibrium position of the $^3T_{2g}$ surface.

6. Conclusions

In this contribution, we have reviewed our results on the spectroscopy and intramolecular energy relaxation processes of C_{60} in rare gas matrices, while presenting new data and revising or improving some of our previous interpretations. Emphasis has been put on medium effects, which turn out to be important both in the static and the time-re-

Table 4

Wavelengths, frequencies and frequency shifts from origin of the bands belonging to the 786.5 nm progression (Fig. 7, Site I), and to the 792.5 nm progression (Fig. 7, Site II) together with the assignement and frequencies from Ref. 22

λ , nm	ν, cm^{-1}	Δν, cm^{-1}	Assignment	Ref. 22
Site I				
788.5	12714	0	origin	–
803.3	12448	266	$h_g(1)$	262
820.9	12182	532	$2h_g(1)$	–
833.1	12004	710	$t_{2u}(2)$	714
834.9	11977	737	$h_u(3)$	743
837.3	11943	771	$h_g(4)$	776
839.2	11916	798	$3h_g(1)$	–
842.2	11873	841	$h_u(4)$	832
850.7	11755	959	$g_u(4)$	961
854.2	11707	1007	$h_u(3) + h_g(1)$	1003
856.4	11667	1037	$h_g(4) + h_g(1)$	1042
861.2	11612	1102	$h_u(4) + h_g(1)$	–
866.4	11542	1172	$t_{1u}(3)$, $t_{2u}(4)$	1204, 1185
877.0	11402	1312	$g_u(5)$	1310
879.0	11376	1338	$h_u(6)$	1342
885.8	11289	1425	$g_u(6)$, $t_{1u}(4)$	1426, 1433
889.2	11246	1468	$h_g(7)$	1477
896.8	11151	1573	$h_g(8)$, $h_u(7)$	1567
906.8	11028	1686	$g_u(6)/t_{1u}(4) + h_g(1)$	–
910.7	10980	1734	$h_g(7) + h_g(1)$	–
919.5	10875	1839	$h_g(8)/h_u(7) + h_g(1)$	–
929.9	10754	1960	$g_u(6)/t_{1u}(4) + 2h_g(1)$	–
Site II				
792.5	12618	0	origin	–
809.3	12357	261	$h_g(1)$	262
827.1	12091	527	$2h_g(1)$	–
844.1	11847	771	$h_g(4)$	776
863.6	11580	1038	$h_g(4) + h_g(1)$	–
884.4	11307	1272	$h_g(6)$	1265
893.0	11198	1420	$g_u(6)$, $t_{1u}(4)$	1426, 1433
904.7	11054	1564	$h_g(8)$, $h_u(7)$	1567
914.7	10932	1686	$g_u(6)/t_{1u}(4) + h_g(1)$	–

solved data. This, in itself, is quite remarkable given the size of C_{60} and its large number of degrees of freedom.

In particular, we have confirmed our previous assignments [22] of the splitting between the lowest three singlet states in absorption and proposed a precise value for their pure electronic origins in the gas phase. In fluorescence, we have discussed the drastic differences between the Ne and Ar data and in particular the change in dominant emitting character from T_{1g} in Ar to T_{2g} in Ne, as well as a similar change between the absorption and the fluorescence data. This was reconciled by assuming different Stokes shifts for the two states, which bring T_{2g} at an energy lower than T_{1g} before emission. A similar situation could occur for the phosphorescence transition to account for the dominant $^3T_{2g}$ character of the phosphorescence data in Xe matrices. We note however that theory predicts it as the lowest triplet state. Both the static and time-resolved fluorescence data indicate strong mixing between the lowest three singlet states, in agreement with their small energy differences. The time-resolved data confirm the nearly degenerate character of the S_1 and S_2 states, while the S_3 state stands slightly above (in the gas phase we inferred an S_1–S_3 splitting of $\sim 100\ cm^{-1}$). In the free molecule, the purely electronic T_{1g} , T_{2g} and G_g levels cannot undergo mixing. Such mixings are induced in the matrix either by static or dynamical crystal field effects which break the I_h symmetry of the molecule. The ultrafast internal conversion process in the singlet state manifold is a remarkable process which deserves further attention and work is in progress to this aim.

Acknowledgments

I would like to thank all my co-workers that have been involved in this work: A Sassara, G. Zerza, M. T. Portella-Oberli, B. Deveaud, J-D. Ganiere. I am also grateful to R. Blades and Z. Al Rahbani for inspiring ideas. This work was supported by the Swiss NSF via contracts 53811.98.

1. Y. Chai, T. Guo, C. Jin, R. E. Haufler, L. P. F. Chibante, J. Fure, J. M. Alford, and R. E. Smalley, *J. Phys. Chem.* **95**, 7564 (1991).
2. B. A. DiCamillo, R. L. Hettich, G. Guiochon, R. M. Compton, M. Saunders, H. A. Jimenez-Vazquez, A. Khong, and R. J. Cross, *J. Phys. Chem.* **100**, 9127 (1996) and Refs. therein.
3. H. Sprang, A. Mahlkow, and E. E. B. Campbell, *Chem. Phys. Lett.* **227**, 91 (1994).
4. L. W. Tutt and A. Kost, *Nature* **356**, 225 (1992).
5. K. Dou, J. Y. Du, and E. T. Knobbe, *J. Lumin.* **83**, 241 (1999).

6. V. M. Farzdinov, Yu. E. Lozovik, Yu. A. Matveets, A. G. Stepanov, and V. S. Letokhov, *J. Phys. Chem.* **98**, 3290 (1994).
7. F. Negri, G. Orlandi, and F. Zerbetto, *Chem. Phys. Lett.* **144**, 31 (1988).
8. F. Negri, G. Orlandi, and F. Zerbetto, *J. Chem. Phys.* **97**, 6496 (1992).
9. F. Negri, G. Orlandi, and F. Zerbetto, *J. Phys. Chem.* **100**, 10849 (1996).
10. F. Negri and G. Orlandi, *J. Phys.* **B29**, 5049 (1996).
11. C. Cepek, A. Goldoni, S. Modesti, F. Negri, G. Orlandi, and F. Zerbetto, *Chem. Phys. Lett.* **250**, 537 (1996).
12. S. Leach, M. Vervloet, A. Despres, E. Bréheret, J. P. Hare, T. J. Dennis, H. W. Kroto, R. Taylor, and D. R. M. Walton, *Chem. Phys.* **160**, 451 (1992).
13. Y.-P. Sun, P. Wang, and N. B. Hamilton, *J. Am. Chem. Soc.* **115**, 6378 (1993).
14. D. J. van den Heuvel, G. J. B. van den Berg, E. J. J. Groenen, J. Schmidt, I. Holleman, and G. Meier, *J. Phys. Chem.* **99**, 11644 (1995).
15. D. J. van den Heuvel, I. Y. Chan, E. J. J. Groenen, M. Matsushita, J. Schmidt, and G. Meijer, *Chem. Phys. Lett.* **223**, 284 (1995).
16. X. L. R. Dauw, M. V. Bronsveld, A. Kruger, J. B. M. Warntjes, M. R. Witjes, and E. J. J. Groenen, *J. Chem. Phys.* **109**, 9332 (1998).
17. J. Feldmann, R. Fischer, E. O. Gobel, and R. Schmitt-Rink, *Phys. Status Solidi* **173**, 339 (1992).
18. M. Muccini, R. Danieli, R. Zamboni, C. Taliani, H. Mohn, W. Muller, and H. U. van ter Meer, *Chem. Phys. Lett.* **245**, 107 (1995).
19. R. E. Haufler, Y. Chai, L. P. F. Chibante, M. R. Froehlich, M. R. Weisman, R. F. Curl, and R. E. Smalley, *J. Chem. Phys.* **95**, 2196 (1991).
20. Z. Gasyna, P. N. Schatz, J. P. Hare, T. J. Dennis, H. W. Kroto, R. Taylor, and D. R. M. Walton, *Chem. Phys. Lett.* **183**, 283 (1991).
21. A. Sassara, G. Zerza, and M. Chergui, *J. Phys.* **B29**, 4997 (1996).
22. A. Sassara, G. Zerza, M. Chergui, F. Negri, and G. Orlandi, *J. Chem. Phys.* **107**, 8731 (1997).
23. A. Sassara, G. Zerza, and M. Chergui, *J. Phys. Chem.* **A102**, 3072 (1998).
24. A. Sassara, G. Zerza, and M. Chergui, *Chem. Phys. Lett.* **261**, 213 (1996).
25. A. Sassara, G. Zerza, M. Chergui, V. Ciulin, J.-D. Ganiere, and B. Deveaud, *J. Chem. Phys.* **111**, 689 (1999).
26. A. Sassara, G. Zerza, V. Ciulin, M. T. Portella-Oberli, J.-D. Ganiere, B. Deveaud, and M. Chergui, *J. Lumin.* **83/84**, 29 (1999).
27. J. D. Close, F. Federmann, K. Hoffmann, and N. Quaas, *Chem. Phys. Lett.* **276**, 393 (1997).
28. M. T. Portella-Oberli, A. Spiridon, F. Vigliotti, A. Sassara, and M. Chergui (work in progress).
29. L. László and L. Udvardi, *Chem. Phys. Lett.* **186**, 418 (1987).
30. R. V. Bensasson, T. Hill, C. Lambert, E. J. Land, S. Leach, and T. G. Truscott, *Chem. Phys. Lett.* **201**, 326 (1993).